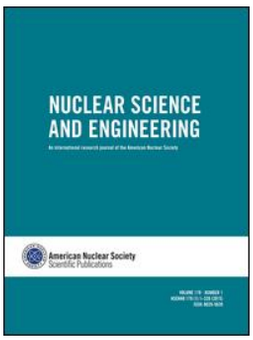

Nuclear Science and Engineering

ISSN: 0029-5639 (Print) 1943-748X (Online) Journal homepage: https://www.tandfonline.com/loi/unse20

A Two-Grid Acceleration Scheme for the Multigroup S_n Equations with Neutron Upscattering

B. T. Adams & J. E. Morel

To cite this article: B. T. Adams & J. E. Morel (1993) A Two-Grid Acceleration Scheme for the Multigroup S_n Equations with Neutron Upscattering, Nuclear Science and Engineering, 115:3, 253-264, DOI: 10.13182/NSE115-253

To link to this article: https://doi.org/10.13182/NSE115-253

Published online: 13 May 2017.

NUCLEAR SCIENCE AND ENGINEERING: 115, 253–264 (1993)

A Two-Grid Acceleration Scheme for the Multigroup S_n Equations with Neutron Upscattering

B. T. Adams* and J. E. Morel

University of California, Los Alamos National Laboratory, Los Alamos, New Mexico 87545

Received October 20, 1992
Accepted June 14, 1993

Abstract—*A two-grid acceleration scheme for the multigroup S_n equations with neutron upscattering is developed. Although it has been tested only in one-dimensional slab geometry with linear-discontinuous spatial differencing, previous experience suggests that it should be applicable in any geometry with any spatial differencing scheme for which an unconditionally efficient diffusion-synthetic acceleration scheme exists. The method is derived, theoretically analyzed, and computationally tested. The results indicate that the scheme is unconditionally effective in terms of error reduction per iteration and highly efficient in terms of computational cost.*

I. INTRODUCTION

The standard outer-iteration scheme used to solve the multigroup S_n equations is the Gauss-Seidel scheme. In the absence of upscattering (i.e., scattering in which a particle gains energy), the Gauss-Seidel method yields the exact flux solution in a single iteration. However, if there is upscattering and a low probability for particle absorption or leakage, the convergence rate of this iterative process can become arbitrarily slow. For instance, it is well known within the reactor physics community that the Gauss-Seidel outer-iteration scheme used in standard multigroup S_N and diffusion codes converges very slowly for neutronics problems with several thermal groups and heavy-water or graphite moderators. Thus, convergence acceleration is highly desirable for such problems.

To our knowledge, the only upscatter acceleration techniques currently employed in the reactor physics community are group-dependent rebalance methods such as that employed in the ONETRAN code.[1] The effectiveness of these schemes is strongly problem dependent, and they often fail on precisely those problems for which convergence acceleration is most needed.

We have developed a two-grid acceleration scheme for the multigroup S_n equations with neutron upscattering. Our theoretical and computational results indicate that this scheme gives rapid convergence rates at a cost per iteration that is very little more than that of the unaccelerated scheme. Although we explicitly consider only source calculations here, our method can also be applied in conjunction with inverse power iteration in eigenvalue calculations. This follows from the fact that each inverse power iteration requires the solution of an effective source problem. Our scheme is very similar in spirit to both the linear multifrequency-grey technique[2] used to accelerate the reemission source in radiative transfer calculations and the S_N fission-source acceleration technique of Morel and McGhee.[3] Our scheme is also somewhat similar to an S_n upscatter acceleration technique very recently developed by Averin and Voloschenko.[4] In particular, our respective schemes are similar in that a one-group diffusion equation is used to estimate the error in the S_n solution iterate. However, our respective schemes differ in that we use a theoretically derived multigroup weight vector to calculate the group-averaged diffusion coefficients and cross sections for the one-group diffusion equation, whereas Averin and Voloschenko use either a nonlinear procedure whereby the multigroup weight vector is taken from the latest S_n solution iterate, or a linear procedure whereby the multigroup weight vector is arbitrarily

*Current address: Phillips Laboratory, PL/VTPN, Kirtland Air Force Base, New Mexico 87117.

assumed to give equal weight to each group. In addition, only the scalar fluxes are accelerated in our scheme, whereas Averin and Voloschenko accelerate both the scalar fluxes and the currents in their scheme. We later show that there is nothing to be gained by accelerating the currents associated with the thermal neutron scattering operator. Averin and Voloschenko consider a more general problem than we do, and this is presumably why they choose to accelerate the currents.

The remainder of this paper is organized as follows. In Sec. II, we describe our two-grid method. In Sec. III, we use Fourier analysis to predict its effectiveness. Computational results are presented in Sec. IV, and conclusions and recommendations for further study are given in Sec. V.

II. THE TWO-GRID METHOD

In one-dimensional slab geometry, the multigroup transport equation is given by

$$\mu \frac{\partial \Psi_g(\mu)}{\partial x} + \sigma_{t,g}\Psi_g(\mu) = \sum_{l=0}^{L} \frac{2l+1}{4\pi}\left(\sum_{g'=1}^{N} \sigma_{s,g'\to g,l}\phi_{g',l} + Q_{g,l}\right)P_l(\mu) , \quad g = 1,N , \quad (1)$$

where

g = energy group index

N = number of energy groups

μ = cosine of the polar angle

$\Psi_g(\mu)$ = neutron angular flux for group g

$\sigma_{t,g}$ = macroscopic total cross section for group g

$\sigma_{s,g'\to g}(\mu_0)$ = macroscopic differential scattering cross section for scattering from group g' to group g

$Q_g(\mu)$ = distributed source for group g

$P_l(\mu)$ = Legendre polynomial of degree l

$\sigma_{s,g'\to g,l}$ = l'th Legendre moment of the macroscopic differential scattering cross section for scattering from group g' to group g.

Also,

$$\sigma_{s,g'\to g,l} = 2\pi \int_{-1}^{1} \sigma_{s,g'\to g}(\mu_0)P_l(\mu_0)\, d\mu_0 ; \quad (2)$$

$\phi_{g',l}$ denotes the l'th Legendre moment of the angular flux for group g:

$$\phi_{g',l} = 2\pi \int_{-1}^{1} \Psi_{g'}(\mu')P_l(\mu')\, d\mu' , \quad (3)$$

and $Q_{g,l}$ denotes the l'th Legendre moment of the distributed source for group g:

$$Q_{g,l} = 2\pi \int_{-1}^{1} Q_g(\mu)P_l(\mu)\, d\mu . \quad (4)$$

Note that the spatial dependence of the flux and the cross sections is suppressed in Eq. (1). Furthermore, since upscatter occurs only between thermal groups, we assume for simplicity that all of the groups in Eq. (1) are thermal. The influence of any suprathermal groups on the thermal groups results from downscatter sources. These sources are implicitly represented by the thermal inhomogeneous source term.

The Gauss-Seidel iterative method is the standard technique for solving Eq. (1), and it can be described as follows:

$$\mu \frac{\partial \Psi_g^{k+1}(\mu)}{\partial x} + \sigma_{t,g}\Psi_g^{k+1}(\mu) = \sum_{l=0}^{L} \frac{2l+1}{4\pi}\left(\sum_{g'=1}^{g} \sigma_{s,g'\to g,l}\phi_{g',l}^{k+1} + \sum_{g'=g+1}^{N} \sigma_{s,g'\to g,l}\phi_{g',l}^{k} + Q_{g,l}\right)P_l(\mu), \quad g = 1,N , \quad (5)$$

where k is the iteration index. Note that in the absence of upscattering, the Gauss-Seidel equations yield the exact solution in a single iterate. By subtracting Eq. (5) from Eq. (1), an exact equation for the error in the Gauss-Seidel iterate is obtained:

$$\mu \frac{\partial \epsilon_g^{k+1}(\mu)}{\partial x} + \sigma_{t,g}\epsilon_g^{k+1}(\mu) = \sum_{l=0}^{L} \frac{2l+1}{4\pi}\left(\sum_{g'=1}^{N} \sigma_{s,g'\to g,l}\epsilon_{g',l}^{k+1} + R_{g,l}^{k+1}\right)P_l(\mu) , \quad (6)$$

where

$$\epsilon_g^{k+1}(\mu) = \Psi_g(\mu) - \Psi_g^{k+1}(\mu) ,$$

$$\epsilon_{g',l}^{k+1} = 2\pi \int_{-1}^{1} \epsilon_{g'}^{k+1}(\mu')P_l(\mu')\, d\mu' ,$$

and

$$R_{g,l}^{k+1} = \sum_{g'=g+1}^{N} \sigma_{s,g'\to g,l}(\phi_{g',l}^{k+1} - \sigma_{g',l}^{k}) .$$

The error associated with the Gauss-Seidel iterate (and hence the exact solution) can be obtained by solving this equation. However, this is not practical since this equation is no easier to solve than the exact multigroup transport equation. The central idea behind the two-grid method is to solve a coarse-grid approximation to this equation and obtain an economical yet accurate estimate of the error. The convergence of the

iteration process is accelerated by adding this error estimate to the flux iterate.

We have performed infinite-medium Fourier analyses for the Gauss-Seidel iteration operators corresponding to each of several materials. The P_1 cross sections for these materials were obtained from a Los Alamos National Laboratory (LANL) 69-group neutron cross-section library[5] containing 41 thermal groups. Our Fourier analyses are described in Sec. III. These analyses yielded two main results. The first result is that the error reduction factor per iteration (the spectral radius) is 0.9998 for heavy water, 0.998 for graphite, and 0.61 for iron. These spectral radii are consistent with the experience of the reactor physics community in that upscatter iterations are known to converge very slowly in heavy water and graphite but reasonably well in other materials such as iron. The second result is that the most poorly attenuated error modes are nearly constant in space, nearly isotropic in angle, and nearly fixed in spectral shape. This fixed spectral shape is exactly Maxwellian if the unaccelerated spectral radius is unity.

If our acceleration scheme is to be effective, the coarse-grid approximation to Eq. (6) must be very accurate for the persistent error modes. The angular and spectral shapes of these modes revealed by Fourier analysis suggest a one-group diffusion approximation for the coarse-grid operator. We can expect that such an operator will indeed accurately estimate the persistent error modes. However, it is important to realize that an accurate estimate of the persistent error modes is *necessary* but not *sufficient* to ensure an effective acceleration scheme. For instance, if the coarse-grid operator is accurate for the persistent modes, it can hardly be expected to be accurate for all the other modes since it is of much lower dimension than the fine-grid operator. It follows that the coarse-grid operator will either underestimate or overestimate many of the nonpersistent error modes. Underestimation of these error modes causes no problems, but overestimation can cause these modes to be amplified. This amplification can be reversed by means of additional relaxation iterations, but this can obviously degrade the efficiency of the overall acceleration scheme. It is essentially impossible to intuitively predict what effect a given coarse-grid operator will have on the well-attenuated error modes. Usually one must simply choose a coarse-grid operator based on its accuracy for the persistent error modes and then perform a Fourier analysis to determine its effect on the nonpersistent modes.

We now proceed to derive our coarse-grid equation. The first step is to approximate Eq. (6) with a multigroup diffusion equation:

$$-\nabla\cdot D_g\nabla\epsilon_{g,o}^{k+1}+\sigma_{t,g}\epsilon_{g,o}^{k+1}=\sum_{g'=1}^{N}\sigma_{s,g'\to g,o}\epsilon_{g',o}^{k+1}+R_{g,o}^{k+1}\ , \quad g=1,N\ , \tag{7}$$

where D_g is the diffusion coefficient for group g:

$$D_g=\frac{1}{3(\sigma_{t,g}-\sigma_{g,1})}\ . \tag{8}$$

We next assume that the solution of this error equation is given by the product of a space-dependent modulation function $E(x)$ and a spectral shape function ξ_g:

$$\epsilon_{g,o}^{k+1}(x)=E(x)\xi_g\ , \tag{9}$$

where

$$\sum_{g=1}^{N}\xi_g=1\ . \tag{10}$$

As one would except, this spectral shape function corresponds to the spectral shape of the persistent error modes. In Sec. III, we show that this shape function is obtained by calculating an eigenvector of a certain matrix constructed from the P_0 multigroup cross-section coefficients. This calculation can easily be carried out using standard mathematical library routines, and it must be carried out for each material in the problem. Substituting from Eq. (9) into Eq. (7) and integrating over all energies (summing over all groups), we obtain the following coarse-grid equation:

$$-\nabla\cdot[\langle D\rangle\nabla E(x)+\langle \boldsymbol{D}\rangle E(x)]+\langle\sigma_a\rangle E(x)=\langle R\rangle\ , \tag{11}$$

where

$$\langle D\rangle=\sum_{g=1}^{N}D_g\xi_g\ , \tag{12}$$

$$\langle \boldsymbol{D}\rangle=\sum_{g=1}^{N}D_g\nabla\xi_g\ , \tag{13}$$

$$\langle\sigma_a\rangle=\sum_{g=1}^{N}\left(\sigma_{t,g}\xi_g-\sum_{g'=1}^{N}\sigma_{s,g'\to g,o}\xi_{g'}\right)\ , \tag{14}$$

and

$$\langle R\rangle=\sum_{g=1}^{N}R_{g,o}^{k+1}\ . \tag{15}$$

Note that Eq. (11) is not a standard diffusion equation because of the term containing the gradient of the shape function. This term is identically zero in homogeneous regions, but it is nonzero in inhomogeneous regions and makes Eq. (11) incompatible with most diffusion solution techniques. Most importantly, it is mathematically undefined at material interfaces. This term is an artifact of our assumption that the spectral shape function depends only on the material cross sections. This is a reasonable assumption at points far from boundaries in homogeneous regions, but it is nonphysical at material interfaces because it leads to a spatially discontinuous shape function. To deal with these difficulties, we simply drop the term containing the gradient of the spectral shape function. The justification for this step follows solely from the effectiveness of the resulting acceleration scheme when it is applied to inhomogeneous

problems. Our scheme is shown to be effective for such problems in Sec. IV. Simplifying Eq. (11), we obtain the final form of the coarse-grid error equation as

$$-\nabla\cdot\langle D\rangle\nabla E(x) + \langle\sigma_a\rangle E(x) = \langle R\rangle \ . \qquad (16)$$

The one-group diffusion coefficient and the absorption cross section in Eq. (16) must be positive to ensure stability in the solution process. It follows from Eqs. (12) and (14) that these quantities will be positive if the spectral shape function is strictly positive. Our experience indicates that the spectral shape function is strictly positive. However, we can prove positivity only if the unaccelerated infinite-medium spectral radius for a given material is identically unity. As previously noted, the spectral shape function is exactly Maxwellian in this case.

We now give the complete equations for our accelerated iteration scheme. An accelerated iteration is begun by performing a Gauss-Seidel iteration sweep on the fine grid (the S_N equations for the thermal groups):

$$\mu\frac{\partial\Psi_g^{k+1/2}(\mu)}{\partial x} + \sigma_{t,g}\Psi_g^{k+1/2}(\mu) = \sum_{l=0}^{L}\frac{2l+1}{4\pi}\left(\sum_{g'=1}^{g}\sigma_{s,g'\to g,l}\phi_{g',l}^{k+1/2} + \sum_{g'=g+1}^{N}\sigma_{s,g'\to g,l}\phi_{g',l}^{k} + Q_{g,l}\right)P_l(\mu), \quad g=1,N \ , \qquad (17)$$

where a half-integral iteration index has been used in anticipation of a two-step process. The isotropic component of the residual $R_{g,o}^{k+1/2}$ is next calculated:

$$R_{g,o}^{k+1/2} = \sum_{g'=g+1}^{N}\sigma_{s,g'\to g,o}(\sigma_{g',0}^{k+1/2} - \phi_{g',0}^{k}) \ , \quad g=1,N \ . \qquad (18)$$

Note that this step is equivalent to calculating the full residual and then projecting it onto the coarse (isotropic) angular grid associated with all diffusion approximations. The projection of the residual onto the coarse one-group diffusion grid is then completed by summing the isotropic component of the residual over all thermal groups:

$$\langle R\rangle = \sum_{g=1}^{N} R_{g,o}^{k+1/2} \ . \qquad (19)$$

The coarse-grid equation is then solved for the energy-integrated scalar flux error estimate:

$$-\nabla\cdot\langle D\rangle\nabla E(x) + \langle\sigma_a\rangle E(x) = \langle R\rangle \ . \qquad (20)$$

Next, the coarse-grid scalar flux error estimate is interpolated onto the fine energy grid by means of the spectral shape function:

$$\tilde{\epsilon}_{g,o}^{k+1/2}(x) = \xi_g E(x) \ . \qquad (21)$$

Finally, the fine-grid scalar flux error estimate is added to the isotropic component of the Gauss-Seidel iterate to obtain the accelerated scalar flux iterate:

$$\phi_{g,o}^{k+1} = \phi_{g,o}^{k+1/2} + \tilde{\epsilon}_{g,o}^{k+1/2} \ . \qquad (22)$$

This completes one accelerated iteration. Note that only the isotropic component of the flux is being accelerated in our scheme. In the Appendix, it is shown that the anisotropic components of the flux are strongly attenuated by a Gauss-Seidel iteration. Therefore, one need only accelerate the isotropic flux component. However, in time-dependent calculations, it can nonetheless be useful to correct the currents to achieve particle balance after each accelerated iteration. A full discussion of this subject is given in Ref. 3 within the context of a fission-source acceleration scheme. The same principles apply to our upscatter scheme. One need not truly accelerate the currents in the sense of including a full P_1 approximation to the error equation. Rather, one can use the diffusion approximation that we have defined and calculate the current corrections in accordance with that approximation:

$$\phi_{g,1}^{k+1} = \phi_{g,1}^{k+1/2} - D_g\xi_g\frac{\partial E}{\partial x} \ . \qquad (23)$$

The interpolation step given by Eq. (21) is not defined at material interfaces. The need for interface interpolation depends entirely on the details of the spatial-differencing scheme being used. For instance, in the linear-discontinuous scheme, the scalar fluxes are assumed to have the following dependence within spatial cell i:

$$\phi(x) = \phi_{i,L}\frac{(x_{i+1/2}-x)}{h_i} + \phi_{i,R}\frac{(x-x_{i-1/2})}{h_i} \ , \qquad (24)$$

where

$\phi_{i,L}, \phi_{i,R}$ = scalar fluxes at the left and right edges of cell i, respectively

$x_{i-1/2}, x_{i+1/2}$ = left and right coordinates of cell i, respectively

h_i = width of cell i.

This dependence is also assumed in the linear-discontinuous diffusion-differencing scheme. Note that even though these unknowns lie at cell edges, each of them is unambiguously associated with cell i and its spectral shape function. Consequently, there is no need to define the spectral interpolation step at the interfaces. In the diamond-difference scheme, the transport fluxes used in the scattering source lie at cell centers, but the diffusion fluxes lie at cell edges. In this case, one first averages the edge diffusion fluxes to obtain the center diffusion fluxes and then performs the interpolation step on the center diffusion fluxes. We cannot consider

every possible differencing scheme here, but we can formulate one principle that can be used to define the interpolation step at material interfaces should it be necessary: The angular flux along any particular direction should assume the spectral shape of the cell from which it is *exiting*.

III. ANALYSIS

In this section, we discuss the main results from a Fourier analysis, performed for both the standard Gauss-Seidel iteration method and our two-grid accelerated scheme, for the multigroup S_n equations with upscatter. We performed this analysis for both isotropic and linearly anisotropic scattering to validate our use of a diffusion equation rather than a P_1 approximation for our coarse-grid operator. The mathematical details of the analysis are given in the Appendix. The Fourier analysis was performed for infinite homogeneous slabs composed of either heavy water, graphite, or iron. A 69-group LANL neutron cross-section library with 41 thermal upscatter groups was used in each case.[5]

The purpose of the Fourier analysis is to calculate the spectral radius of the Gauss-Seidel and the two-grid iterative operators for one-dimensional slab geometry. An infinite homogeneous medium is assumed. To perform the analysis, the iteration equations must be manipulated to relate the flux errors prior to an iteration to the flux errors after an iteration. The differential operator that defines this relationship is called the iteration operator, and its spectral radius determines the asymptotic error reduction factor for the iteration process. The error is assumed to have a spatial dependence of the form $\exp(i\lambda x)$ for $\lambda \in (-\infty,\infty)$, where $i = \sqrt{-1}$. With this assumption, the differential operator reduces to an algebraic matrix operator, called the Fourier matrix, that depends on the Fourier mode parameter λ. The dimensions of the Fourier matrix are determined by the number of upscatter groups present in the cross-section library. The Fourier matrix is 41×41 in our analysis. The eigenvalues of the Fourier matrix are the eigenvalues of the iteration operator that correspond to the spatial Fourier mode defined by λ. We denote them by $\{\omega_g(\lambda)\}_{g=1}^{41}$. Standard library routines can be used to compute these eigenvalues for any value of λ. We define the modal spectral radius as the spectral radius corresponding to a specific Fourier mode:

$$\rho_M(\lambda) = \max\{|\omega_g(\lambda)|\}_{g=1}^{41} . \quad (25)$$

The spectral radius of the iteration operator is the maximum of the modal spectral radii:

$$\rho = \max\{\rho_M(\lambda)\} , \quad \text{for all } \lambda . \quad (26)$$

In Figs. 1, 2, and 3, the modal spectral radii of the Gauss-Seidel and the two-grid iteration matrices are plotted as a function of λ for heavy water, graphite, and iron, respectively. These curves were generated from the Fourier analysis performed with isotropic scattering. Only the values for positive λ are plotted since the modal spectral radius is an even function of λ. We have determined by extensive numerical evaluation that the modal spectral radius is a monotonically decreasing function of λ for all three iteration operators and that the spectral radius of each operator corresponds to the $\lambda = 0$ Fourier mode. This finding is reflected in Figs. 1, 2, and 3. For those errors that vary slowly in space (i.e., small values of λ), the modal spectral radii of the two-grid scheme are smaller than the corresponding radii of the Gauss-Seidel operator in each material. This indicates that our acceleration scheme effectively attenuates these error components. At higher

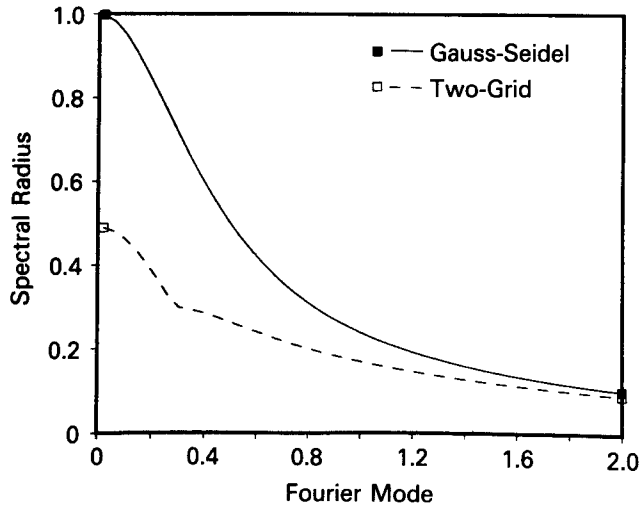

Fig. 1. Modal spectral radii for heavy water.

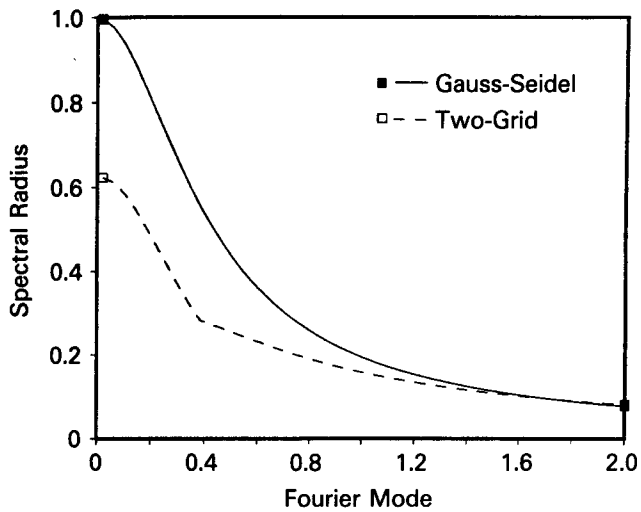

Fig. 2. Modal spectral radii for graphite.

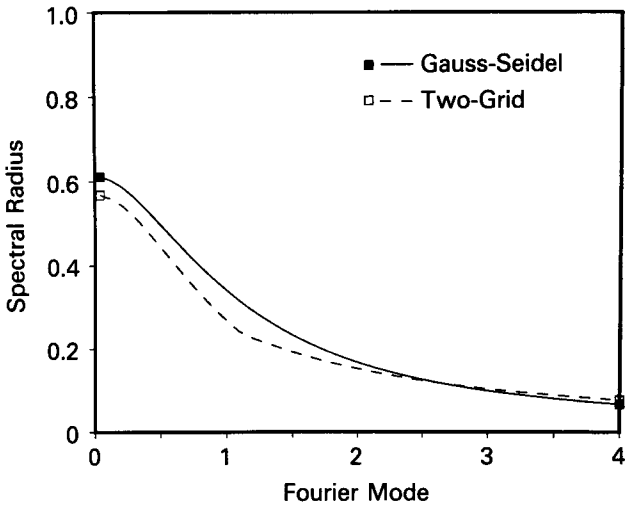

Fig. 3. Modal spectral radii for iron.

frequencies, the two-grid modal spectral radii exceed the corresponding Gauss-Seidel radii in some cases, although the effect is small. These error components are strongly attenuated by both methods. Therefore, significant error amplification does not occur.

The spectral radii of the Gauss-Seidel and the two-grid iterative operators with isotropic scattering are given for each material in Table I. The inclusion of linearly anisotropic scattering has a negligible effect on the spectral radius of either method. We analyzed the spectral radius of both methods for the linearly anisotropic case and found no significant differences from the isotropic case. Consequently, we elected to accelerate only the isotropic component of the flux in our two-grid scheme. The insensitivity of the spectral radii to the linearly anisotropic component of the scattering cross section justifies our neglect of the higher-order flux moments. Note that the spectral radius of the Gauss-Seidel operator is very close to unity for infinite media composed of either heavy water or graphite. The spectral radius of our two-grid operator is significantly smaller in these materials, which indicates that the computational effort required to solve the multigroup transport equations in these materials will also be significantly reduced. For instance, in excess of 11 000 iterations of the Gauss-Seidel method would be required to reduce the error by an order of magnitude for an infinite medium composed of heavy water, but our two-grid method would require only about three iterations to similarly reduce the error. The two-grid method does not yield a significant improvement in iron. However, the standard Gauss-Seidel process is effective in this material, so acceleration is not required.

TABLE I

Spectral Radius of Gauss-Seidel and Two-Grid Methods

Material	Gauss-Seidel	Two-Grid
Heavy water	0.9998	0.4886
Graphite	0.9984	0.6219
Iron	0.6120	0.5686

It is appropriate to ask why our scheme is so effective in two materials but marginally effective in a third. The key to this question lies in the distribution of the eigenvalues arising from the Fourier matrix at $\lambda = 0$ for the Gauss-Seidel iteration scheme. As previously discussed, the Gauss-Seidel spectral radius arises from the $\lambda = 0$ matrix in all three materials. Our one-group diffusion approximation to the error equation is designed to be exact for the $\lambda = 0$ error mode associated with the Gauss-Seidel spectral radius, but it is not clear that it should necessarily be accurate for any of the other modes associated with the $\lambda = 0$ matrix. In fact, we have numerically determined that the acceleration step has no effect on these other modes. This is reflected in the fact that the *accelerated* spectral radius in all three materials is equal to the *second-largest* eigenvalue of the Gauss-Seidel Fourier matrix at $\lambda = 0$. Our scheme is extremely effective in heavy water and graphite because both of these materials have a second-largest Gauss-Seidel eigenvalue at $\lambda = 0$, which is much smaller than the largest eigenvalue. Our scheme is marginally effective in iron because it has a second-largest Gauss-Seidel eigenvalue at $\lambda = 0$, which is only slightly less than the largest eigenvalue. In particular, the largest eigenvalues for heavy water, graphite, and iron are 0.9998, 0.9984, and 0.6120, respectively, while the second-largest are 0.4886, 0.6219, and 0.5686, respectively. Note that these second-largest eigenvalues are equal to the accelerated spectral radius values given in Table I. Thus, we can state that our two-grid scheme is very effective for heavy water and graphite only because the Gauss-Seidel Fourier matrix at $\lambda = 0$ has a largest eigenvalue that is *isolated* from the other eigenvalues. This is a very fortuitous result. If the eigenvalues were uniformly distributed between zero and unity (which is often the case for discretizations of differential operators), our two-grid scheme would not be effective for these materials since more than one error mode at $\lambda = 0$ would need to be attenuated. A multigrid method rather than a two-grid method would be required to attenuate several error modes at $\lambda = 0$.

Previous community-wide experience indicates that one should not expect a Fourier analysis for the spatially differenced S_n equations to give a spectral radius significantly larger than that for the spatially analytic equations as long as the multigroup transport equations and the one-group diffusion equation are consistently differenced. If any differences were to occur, they would arise with spatial cells of intermediate or large optical thicknesses. We have not observed any detrimental thick-cell effects while computationally testing

our method. Our computational results are discussed in Sec. IV.

The Fourier matrices of the Gauss-Seidel and the two-grid iterative methods are developed in the Appendix. In each case, the spectral radius corresponds to the $\lambda = 0$ Fourier mode of the iteration matrix. Assuming isotropic scattering in an infinite homogeneous medium, the spectral radius of the Gauss-Seidel iteration matrix is determined from the eigenvalue problem:

$$(\mathbf{T} - \mathbf{S}_{Do})^{-1}\mathbf{S}_{Uo}\boldsymbol{\xi} = \rho\boldsymbol{\xi} \ , \qquad (27)$$

where

$\mathbf{T}$ = total cross-section matrix

$\mathbf{S}_{Do}$ = isotropic downscatter matrix

$\mathbf{S}_{Uo}$ = isotropic upscatter matrix

ρ = spectral radius

$\boldsymbol{\xi}$ = corresponding eigenvector.

In our accelerated iteration scheme, this eigenvector is used to interpolate the coarse-grid error estimate onto the fine grid. Thus, this eigenvalue problem must be solved for each homogeneous material region in the problem prior to beginning the iterative process. The eigenvalue problems that allow the determination of the modal spectral radius for each method are fully developed in the Appendix. In Sec. IV, the spectral radii of the Gauss-Seidel and the two-grid methods are computationally estimated and compared with our theoretical predictions.

IV. COMPUTATIONAL RESULTS

In this section, we present the results of a series of calculations that we performed with our two-grid method. We compare the two-grid scheme with the standard Gauss-Seidel iterative procedure and the whole-system group-dependent rebalance technique used in the ONETRAN code.[1] The spatial differencing of both the multigroup transport equation and the one-group diffusion equation was performed using a linear-discontinuous approximation. The diffusion differencing is fully consistent with the S_n differencing. As previously discussed, consistent spatial differencing of the transport and diffusion equations should ensure that the two-grid method will be effective in real calculations, regardless of the actual spatial-differencing scheme that is used.

All calculations were performed on a Cray-XMP computer. A 69-group cross-section library with P_3 scattering and 41 upscatter groups was used in each case.[5] The first three cases consider homogeneous media composed of either heavy water, graphite, or iron. These problems are intended to simulate an infinite medium and, thus, allow a comparison between the theoretical and computational spectral radii. They are also problems for which the rebalance method (assuming a spatially constant initial flux guess) gives an exact solution in one iteration. These calculations correspond to the following problem:

1. one-dimensional slab geometry
2. spatially constant, isotropic distributed source in energy group 1
3. reflective boundary conditions at left and right faces
4. S_4 with fourth-order Gauss quadrature set
5. ten spatial cells
6. relative scalar flux convergence tolerance of 10^{-4}
7. slab thickness of 10 spectrum-averaged mean free paths (mfp), where such an mfp is equal to three times the one-group diffusion coefficient defined by Eq. (12).

The fourth case considered consists of 10 spectrum-averaged mfp each of carbon, heavy water, and iron in a single slab. This calculation is intended to demonstrate the validity of the two-grid approach for problems with multiple materials. The specified materials simulate the moderator, coolant, and clad of an arbitrary fuel lattice. This calculation corresponds to the following problem:

1. one-dimensional slab geometry
2. isotropic surface source in energy group 1 on right face
3. reflective boundary conditions at left face
4. S_4 Gauss quadrature set
5. ten spatial cells per material
6. relative scalar flux convergence tolerance of 10^{-4}
7. slab thickness of 30 spectrum-averaged mfp (10 mfp/material).

The spectral radius for each of our calculations with the Gauss-Seidel and the two-grid methods was computationally estimated as follows:

$$\rho^{k+1} = \left[\frac{\sum_{all\ i,g} (\phi_{i,g}^{k+1} - \phi_{i,g}^{k})^2}{\sum_{all\ i,g} (\phi_{i,g}^{k} - \phi_{i,g}^{k-1})^2} \right]^{1/2} , \qquad (28)$$

where $\phi_{i,g}^{k+1}$ denotes the scalar flux iterate at step $k+1$ for spatial cell i and energy group g. The spectral radius is not defined for the rebalance method because it is a nonlinear method.

The performance of our two-grid scheme is compared with the Gauss-Seidel and the rebalance schemes in Table II. The computational spectral radii of both

TABLE II

Performance of Gauss-Seidel, Rebalance, and Two-Grid Methods

Iterative Scheme	Material	Computational Spectral Radius	Theoretical Spectral Radius	Iterations Required	CPU Time (s)
GS	Heavy water	0.9998	0.9998	45 819	113 742
RB	Heavy water	---	---	2	5.5
TG	Heavy water	0.4825	0.4886	9	22
GS	Graphite	0.9984	0.9984	5 811	14 525
RB	Graphite	---	---	2	5.5
TG	Graphite	0.6194	0.6219	16	39
GS	Iron	0.6121	0.6121	30	74
RB	Iron	---	---	2	5.7
TG	Iron	0.5686	0.5686	28	69
GS	All three	0.9943	---	1 648	16 843
RB	All three	---	---	356	3 627
TG	All three	0.6091	---	21	210

the Gauss-Seidel and the two-grid methods for the infinite-medium problems show excellent agreement with theory. As predicted, the two-grid scheme is much more effective than the Gauss-Seidel method for the heavy water, graphite, and iron cases. The Gauss-Seidel scheme requires 45 819, 5811, and 30 iterations for the heavy water, graphite, and iron calculations, respectively, but the two-grid scheme required less than 30 iterations for each of these calculations. For these same calculations, the two-grid scheme is faster by factors of 5170, 372, and 1.07, respectively. The acceleration of the two-grid scheme for the iron case is nominal, but the Gauss-Seidel method is effective in this material, so acceleration is not required. The rebalance scheme gives the exact solution to the infinite-medium problems on the first iteration, but since a minimum of two iterations is required to measure the error, two iterations were required by the rebalance method for each calculation. Although the rebalance method is the best for infinite-medium problems, such problems are of little practical interest. Our only motivation for considering these problems is that they allow a rigorous comparison between theoretical and computational spectral radii for the Gauss-Seidel and the two-grid schemes.

For the three-region problem, the Gauss-Seidel, rebalance, and two-grid schemes required 1648, 356, and 21 iterations, respectively. The two-grid scheme is the most efficient for a space-dependent problem by factors of 80 and 17 relative to the Gauss-Seidel and rebalance schemes, respectively. The two-grid computational spectral radius obtained for this problem was less than the maximum of the spectral radii obtained in the homogeneous infinite-medium problems. Other inhomogeneous problems that we have performed show similar behavior. Thus, it would appear that our decision to neglect the drift term in the grey equation is justified. The spectral radius of the two-grid scheme in multiregion problems appears to be bounded by the maximum of the spectral radii obtained in the corresponding homogeneous infinite-medium problems.

The time required per outer iteration by the various methods can be calculated from the data given in Tables I and II. In some cases, the accelerated schemes show a slightly smaller time per outer iteration than the Gauss-Seidel method. This initially seems impossible since one must do extra work to generate and solve the acceleration equations. However, the inner iterations sometimes converge slightly faster when the outer iterations are accelerated, resulting in a time per outer iteration smaller than that of the unaccelerated scheme.

It is well known that spatial-differencing effects can destabilize the diffusion synthetic scheme. Destabilization arises from a lack of consistency between the spatial differencing of the S_n equations and the spatial differencing of the diffusion equation. To avoid this phenomenon, we used standard linear-discontinuous S_n spatial differencing and a fully consistent linear-discontinuous diffusion differencing recently developed by Wareing.[6] The partially consistent linear-discontinuous diffusion differencing developed by Adams and Martin[7] was also tested and found to be as effective as the fully consistent differencing for the problems that we considered. If destabilization were to occur, it would be expected to occur in problems with cells of either intermediate or large thickness. To investigate the stability of the two-grid scheme, we performed several calculations with cell thicknesses from 0.1 to 100 mfp. We obtained excellent agreement with our analytic Fourier analysis for these problems with both diffusion-differencing schemes. Thus, our computational results show no indication of cell thickness effects for the two-grid scheme.

In closing this section, we note that although coarse-mesh group-dependent rebalance is available in the ONETRAN code,[1] and one might expect the coarse-mesh rebalance method to perform better than a whole-system rebalance method, we decided not to use the coarse-mesh rebalance method in our computational comparisons. This decision was based on two factors. First, the acceleration equations associated with the whole-system rebalance method can be directly solved via Gauss elimination, whereas those associated with the coarse-mesh rebalance method must generally be solved iteratively. Specifically, in the ONETRAN code,[1] the Gauss-Seidel method is used to solve the coarse-mesh group-dependent rebalance equations. If the Gauss-Seidel method is slowly convergent for the multigroup S_n equations, it will also be slowly convergent for the coarse-mesh group-dependent rebalance acceleration equations. Thus, it is clear that the coarse-mesh group-dependent rebalance scheme used in the ONETRAN code[1] cannot compete with our two-grid scheme for the difficult problems we have considered. Second, it is well known that coarse-mesh rebalance methods can become unstable and tend to do so in precisely those problems that most need acceleration. We feel that the uncertainty associated with the stability of coarse-mesh rebalance methods makes them undesirable relative to any scheme that is unconditionally stable and effective.

V. CONCLUSIONS

Our theoretical and computational results indicate that the two-grid scheme is a vastly superior technique for solving the multigroup transport equations with upscattering, in comparison to the standard Gauss-Seidel and the group-dependent whole-system rebalance techniques. The degree of improvement that is obtained with the two-grid scheme is material dependent; a significant improvement was obtained for heavy water and graphite, while the acceleration obtained in iron was nominal. Significant acceleration is not required for iron, however, because the Gauss-Seidel method is quite effective in this material. In the two-grid scheme, the spectral radius of the space-independent Gauss-Seidel iteration matrix is calculated for each material, as part of the cross-section input and preparation, prior to the initiation of the iterative process. Within the transport code, a conditional check of the magnitude of the maximum spectral radius could be made to determine if the two-grid method should be executed.

The two-grid scheme has been developed for one-dimensional slab geometry in this paper, but it appears that the method can be easily generalized to curvilinear and multidimensional geometries. An efficient implementation of the two-grid scheme requires an efficient technique for solving the coarse-grid diffusion equation. The stability of our method was preserved in our calculations by maintaining consistency in the spatial differencing of the S_n and diffusion equation. A consistently differenced diffusion equation cannot always be obtained for multidimensional S_n calculations with advanced (linear-discontinuous or linear-discontinuous-like) differencing. Furthermore, if such an equation is obtained, one may not be able to solve it efficiently. These considerations may limit the applicability of the two-grid method for multidimensional geometries in the immediate future. However, advances in multidimensional diffusion-synthetic acceleration techniques are rapidly being made, and such advances are directly applicable to our two-grid scheme.

APPENDIX

FOURIER ANALYSIS

In this appendix, we present the mathematical details of a Fourier analysis of the Gauss-Seidel and the two-grid methods. This analysis is based on an infinite one-dimensional slab composed of a homogeneous medium. For our 69-group LANL library,[5] the 28 downscatter groups simply supply a distributed source to the 41 thermal upscatter groups. Only the 41 upscatter groups are considered in this analysis (i.e., energy group 1 in this analysis corresponds to group 29 of the cross-section library). To perform the Fourier analysis, one must relate the errors at the beginning of an iteration to the errors at the end of an iteration. Let $\Psi_g(\mu)$ denote the exact angular flux solution of the multigroup transport equation for group g:

$$\mu \frac{\partial \Psi_g(\mu)}{\partial x} + \sigma_{t,g}\Psi_g(\mu) = \sum_{l=0}^{L} \frac{2l+1}{4\pi} \left(\sum_{g'=1}^{g} \sigma_{s,g'\to g,l}\phi_{g',l} + \sum_{g'=g+1}^{N} \sigma_{s,g'\to g,l}\phi_{g',l} + Q_{g,l} \right) P_l(\mu) , \tag{A.1}$$

where the spatial dependence of the flux and cross sections has been suppressed and downscatter and upscatter have been separated. Subtracting the equation for the Gauss-Seidel iterate at step $(k+\frac{1}{2})$, Eq. (A.1), from the exact equation, Eq. (5), yields an equation for the error in the Gauss-Seidel iterate:

$$\mu \frac{\partial \epsilon_g^{k+1/2}(\mu)}{\partial x} + \sigma_{t,g}\epsilon_g^{k+1/2}(\mu) = \sum_{l=0}^{L} \frac{2l+1}{4\pi} \left(\sum_{g'=1}^{g} \sigma_{s,g'\to g,l}\epsilon_{g',l}^{k+1/2} + \sum_{g'=g+1}^{N} \sigma_{s,g'\to g,l}\epsilon_{g',l}^{k} \right) P_l(\mu) , \tag{A.2}$$

where

$$\epsilon_g^{k+1/2}(\mu) = \Psi_g(\mu) - \Psi_g^{k+1/2}(\mu)$$

and

$$\epsilon_{g',l}^{k+1/2} = 2\pi \int_{-1}^{1} \epsilon_{g'}^{k+1/2}(\mu') P_l(\mu')\, d\mu' \ .$$

We assume that the error in any particular iterate for the group fluxes can be expanded in terms of the Fourier basis functions. Specifically, we assume that

$$\epsilon_g^{k+1/2}(x,\mu) = \int_{-\infty}^{+\infty} \epsilon_g^{k+1/2}(\lambda,\mu) e^{i\lambda x}\, d\lambda \ , \quad \lambda \in (-\infty,\infty) \qquad \text{(A.3)}$$

and

$$\epsilon_{g',l}^{k+1/2}(x) = 2\pi \int_{-1}^{1} \epsilon_g^{k+1/2}(\lambda,\mu') e^{i\lambda x} P_l(\mu')\, d\mu' \ . \qquad \text{(A.4)}$$

Assuming the error is composed of a single Fourier mode, we substitute into the multigroup error equation, Eq. (A.2), to obtain

$$\mu i\lambda \epsilon_g^{k+1/2}(\lambda,\mu) + \sigma_{t,g}\epsilon_g^{k+1/2}(\lambda,\mu) = \sum_{l=0}^{L} \frac{2l+1}{4\pi} \left[\sum_{g'=1}^{g} \sigma_{s,g'\to g,l} \epsilon_{g',l}^{k+1/2}(\lambda) + \sum_{g'=g+1}^{N} \sigma_{s,g'\to g,l} \epsilon_{g',l}^{k}(\lambda) \right] P_l(\mu) \ , \qquad \text{(A.5)}$$

or in matrix form,

$$(\mu i\lambda \mathbf{I} + \mathbf{T})\boldsymbol{\epsilon}^{k+1/2}(\lambda,\mu) = \sum_{l=0}^{L} \frac{2l+1}{4\pi} [\mathbf{S}_{Dl}\boldsymbol{\epsilon}_l^{k+1/2}(\lambda) + \mathbf{S}_{Ul}\boldsymbol{\epsilon}_l^{k}(\lambda)] P_l(\mu) \ , \qquad \text{(A.6)}$$

where

$\mathbf{I}$ = identity matrix

$\mathbf{T}$ = diagonal total cross-section matrix

$\boldsymbol{\epsilon}^{k+1/2}(\lambda,\mu)$ = angularly dependent error vector

$\mathbf{S}_{Dl}$ = matrix composed of the l'th-order Legendre expansion coefficients of the downscatter cross sections

$\mathbf{S}_{Ul}$ = corresponding matrix for the upscatter cross sections.

The order of the Legendre expansion must be defined to proceed. Consider first the case of isotropic scattering. Multiplying Eq. (A.6) by $P_0(\mu)$, with $L = 0$, integrating over all directions, and solving for $\epsilon_o^{k+1/2}(\lambda)$ yields an equation for the modal eigenvalues of the Gauss-Seidel Fourier matrix:

$$\boldsymbol{\epsilon}_o^{k+1/2}(\lambda) = \left\{ \left[\mathbf{I} - \frac{1}{\lambda} \tan^{-1}\left(\frac{\lambda}{\mathbf{T}}\right) \mathbf{S}_{Do} \right]^{-1} \times \frac{1}{\lambda} \tan^{-1}\left(\frac{\lambda}{\mathbf{T}}\right) \mathbf{S}_{Uo} \right\} \boldsymbol{\epsilon}_o^{k}(\lambda) \ . \qquad \text{(A.7)}$$

This expression relates the error in the scalar flux vector at iteration step $(k + \frac{1}{2})$ to the error in the scalar flux vector at iteration step (k), assuming that the scattering is isotropic and that the initial error has a spatial dependence of $\exp(i\lambda x)$. The term in braces is the iteration matrix for the Gauss-Seidel process, and its eigenvalues determine the convergence rate of the process for a specific Fourier mode. The eigenvalues of the iteration matrix associated with λ satisfy:

$$\omega(\lambda)\boldsymbol{\epsilon}_o^{k}(\lambda) = \left\{ \left[\mathbf{I} - \frac{1}{\lambda} \tan^{-1}\left(\frac{\lambda}{\mathbf{T}}\right) \mathbf{S}_{Do} \right]^{-1} \times \frac{1}{\lambda} \tan^{-1}\left(\frac{\lambda}{\mathbf{T}}\right) \mathbf{S}_{Uo} \right\} \boldsymbol{\epsilon}_o^{k}(\lambda) \ . \qquad \text{(A.8)}$$

These eigenvalues can be determined using standard library routines. The modal spectral radius is defined as the spectral radius corresponding to a specific Fourier mode, as shown in Eq. (25). The spectral radius of the iteration process is the maximum of the modal spectral radii [Eq. (26)]. By evaluating Eq. (A.8) at many values of λ, we have determined that the spectral radius corresponds to the $\lambda = 0$ Fourier mode. Examining Eqs. (A.5), (A.6), and (A.7), it follows that the spectral radius of the Gauss-Seidel process with isotropic scattering is determined by the eigenvalue problem:

$$\omega(\lambda)\boldsymbol{\epsilon}_o^{k}(0) = (\mathbf{T} - \mathbf{S}_{Do})^{-1}\mathbf{S}_{Uo}\boldsymbol{\epsilon}_o^{k}(0) \ . \qquad \text{(A.9)}$$

This analysis may be extended to the linearly anisotropic case. Multiplying Eq. (A.6) by $P_o(\mu)$, with $L = 1$, and integrating over all directions yields

$$\left[\mathbf{I} - \frac{1}{\lambda} \tan^{-1}\left(\frac{\lambda}{\mathbf{T}}\right) \mathbf{S}_{Do} \right] \boldsymbol{\epsilon}_o^{k+1/2}(\lambda) + \frac{3i}{\lambda} \left[\mathbf{I} - \frac{1}{\lambda} \mathbf{T} \tan^{-1}\left(\frac{\lambda}{\mathbf{T}}\right) \right] \mathbf{S}_{D1} \boldsymbol{\epsilon}_1^{k+1/2}(\lambda) = \frac{1}{\lambda} \tan^{-1}\left(\frac{\lambda}{\mathbf{T}}\right) \mathbf{S}_{Uo} \boldsymbol{\epsilon}_o^{k}(\lambda) - \frac{3i}{\lambda} \left[\mathbf{I} - \frac{1}{\lambda} \mathbf{T} \tan^{-1}\left(\frac{\lambda}{\mathbf{T}}\right) \right] \mathbf{S}_{U1} \boldsymbol{\epsilon}_1^{k}(\lambda) \ . \qquad \text{(A.10)}$$

Similarly, multiplying by $P_1(\mu)$ and integrating over all directions yields

$$\frac{i}{\lambda}\left[\mathbf{I}-\frac{1}{\lambda}\mathbf{T}\tan^{-1}\left(\frac{\lambda}{\mathbf{T}}\right)\right]\mathbf{S}_{Do}\epsilon_o^{k+1/2}(\lambda)+\left\{\mathbf{I}-\frac{3i}{\lambda^2}\mathbf{T}\left[\mathbf{I}-\frac{1}{\lambda}\mathbf{T}\tan^{-1}\left(\frac{\lambda}{\mathbf{T}}\right)\right]\mathbf{S}_{D1}\right\}\epsilon_1^{k+1/2}(\lambda)$$
$$=-\frac{i}{\lambda}\left[\mathbf{I}-\frac{1}{\lambda}\mathbf{T}\tan^{-1}\left(\frac{\lambda}{\mathbf{T}}\right)\right]\mathbf{S}_{Uo}\epsilon_o^{k}(\lambda)+\frac{3i}{\lambda^2}\mathbf{T}\left[\mathbf{I}-\frac{1}{\lambda}\mathbf{T}\tan^{-1}\left(\frac{\lambda}{\mathbf{T}}\right)\right]\mathbf{S}_{U1}\epsilon_1^{k}(\lambda)\ . \quad (A.11)$$

Combining terms and rearranging, one obtains the iteration matrix for the Gauss-Seidel process with linearly anisotropic scattering:

$$\begin{bmatrix}\epsilon_o^{k+1/2}(\lambda)\\ \epsilon_1^{k+1/2}(\lambda)\end{bmatrix}=L_1^{-1}(\lambda)L_2(\lambda)\begin{bmatrix}\epsilon_o^{k}(\lambda)\\ \epsilon_1^{k}(\lambda)\end{bmatrix}\ , \quad (A.12)$$

where

$$L_1(\lambda)=\begin{bmatrix}\left[\mathbf{I}-\frac{1}{\lambda}\tan^{-1}\left(\frac{\lambda}{\mathbf{T}}\right)\mathbf{S}_{Do}\right] & \frac{3i}{\lambda}\left[\mathbf{I}-\frac{1}{\lambda}\mathbf{T}\tan^{-1}\left(\frac{\lambda}{\mathbf{T}}\right)\right]\mathbf{S}_{D1}\\ \frac{i}{\lambda}\left[\mathbf{I}-\frac{1}{\lambda}\mathbf{T}\tan^{-1}\left(\frac{\lambda}{\mathbf{T}}\right)\right]\mathbf{S}_{Do} & \left\{\mathbf{I}-\frac{3}{\lambda^2}\mathbf{T}\left[\mathbf{I}-\frac{1}{\lambda}\mathbf{T}\tan^{-1}\left(\frac{\lambda}{\mathbf{T}}\right)\right]\mathbf{S}_{D1}\right\}\end{bmatrix}$$

and

$$L_2(\lambda)=\begin{bmatrix}\frac{1}{\lambda}\tan^{-1}\left(\frac{\lambda}{\mathbf{T}}\right)\mathbf{S}_{Uo} & -\frac{3i}{\lambda}\left[\mathbf{I}-\frac{1}{\lambda}\mathbf{T}\tan^{-1}\left(\frac{\lambda}{\mathbf{T}}\right)\right]\mathbf{S}_{U1}\\ -\frac{i}{\lambda}\left[\mathbf{I}-\frac{1}{\lambda}\mathbf{T}\tan^{-1}\left(\frac{\lambda}{\mathbf{T}}\right)\right]\mathbf{S}_{Uo} & \frac{3}{\lambda^2}\mathbf{T}\left[\mathbf{I}-\frac{1}{\lambda}\mathbf{T}\tan^{-1}\left(\frac{\lambda}{\mathbf{T}}\right)\right]\mathbf{S}_{U1}\end{bmatrix}\ .$$

The spectral radius of the Gauss-Seidel process with linearly anisotropic scattering can be determined from Eq. (A.12) in a manner analogous to the isotropic analysis, although there are twice as many eigenvalues to be determined for each Fourier mode. This technique could be extended to higher orders of anisotropy, although the mathematics would become cumbersome. However, this is not necessary because one would expect neutron scattering at thermal energies to be weakly anisotropic. Therefore, the isotropic analysis should predict the spectral radius accurately, even when a high-order Legendre expansion is utilized in an actual calculation. The Fourier matrix for both P_0 and P_1 scattering was developed to allow verification of this assumption. By comparing the spectral radius of the isotropic and linearly anisotropic Fourier matrices, the effect of the higher-order moments on the convergence rate of the iterative process may be estimated.

We now proceed to develop the Fourier matrix for our two-grid accelerated scheme. The error in the iterate at step $(k+\frac{1}{2})$ of the multigroup diffusion equation is given by Eq. (7):

$$-\nabla\cdot D_g\nabla\epsilon_{g,o}^{k+1/2}+\sigma_{t,g}\epsilon_{g,o}^{k+1/2}$$
$$=\sum_{g'=1}^{N}\sigma_{s,g'\to g,o}\epsilon_{g',o}^{k+1/2}+R_{g,o}^{k+1/2}\ , \quad (A.13)$$

where the residual is defined from the relation of Eq. (18):

$$R_{g,l}^{k+1/2}=\sum_{g'=g+1}^{N}\sigma_{s,g'\to g,l}(\phi_{g',l}^{k+1/2}-\phi_{g',l}^{k})\ . \quad (A.14)$$

Our method begins with a standard Gauss-Seidel transport iteration on the fine, multigroup energy grid. The second step of the acceleration process is to solve a coarse-grid approximation to Eq. (A.13) for an estimate of the error in the Gauss-Seidel iterate. In the two-grid technique, it is assumed that this error is given by the product of the persistent shape function ξ and a group-integrated error $E(x)$. The group-integrated error and the residual will be expanded in the Fourier basis functions as

$$\epsilon_{g,o}^{k+1/2}(x)=\xi_g E(\lambda)e^{i\lambda x}\ , \qquad \lambda\in(-\infty,\infty) \quad (A.15)$$

and

$$R_{g,o}^{k+1/2}(x)=R_{g,o}^{k+1/2}(\lambda)e^{i\lambda x}\ , \quad \lambda\in(-\infty,\infty)\ . \quad (A.16)$$

Inserting these functions into Eq. (A.13), assuming an infinite homogeneous medium, yields

$$\lambda^2 D_g\xi_g E(\lambda)+\sigma_{t,g}\xi_g E(\lambda)$$
$$=\sum_{g'=1}^{N}\sigma_{s,g'\to g,o}\xi_{g'}E(\lambda)+R_{g,o}^{k+1/2}(\lambda)\ , \quad (A.17)$$

or in matrix form,

$$(\lambda^2\mathbf{D} + \mathbf{T} - \mathbf{S}_{Do} - \mathbf{S}_{Uo})\xi E(\lambda) = \boldsymbol{R}_o^{k+1/2}(\lambda) \ . \tag{A.18}$$

This fine-grid equation is mapped onto the coarse grid using the projection operator $\tilde{P}$. The projection operator integrates the fine-grid equation over all energies. Applying this operator and solving for $E(\lambda)$, we get

$$E(\lambda) = [\tilde{P}(\lambda^2\mathbf{D} + \mathbf{T} - \mathbf{S}_{Do} - \mathbf{S}_{Uo})\xi]^{-1}\tilde{P}\boldsymbol{R}_o^{k+1/2}(\lambda) \ . \tag{A.19}$$

This coarse-grid error estimate is then interpolated onto the fine grid using the interpolation operator ξ and added to the Gauss-Seidel iterate to give the accelerated iterate:

$$\phi_{g,o}^{k+1} = \phi_{g,o}^{k+1/2} + \xi[\tilde{P}(\lambda^2\mathbf{D} + \mathbf{T} - \mathbf{S}_{Do} - \mathbf{S}_{Uo})\xi]^{-1}\tilde{P}\boldsymbol{R}_o^{k+1/2}(\lambda) \ . \tag{A.20}$$

The error in the accelerated iterate is then given by

$$\begin{aligned}\boldsymbol{\epsilon}_o^{k+1}(\lambda) &= \boldsymbol{\phi}_o - \boldsymbol{\phi}_o^{k+1} \\ &= \boldsymbol{\epsilon}_o^{k+1/2}(\lambda) \\ &\quad - \xi[\tilde{P}(\lambda^2\mathbf{D} + \mathbf{T} - \mathbf{S}_{Do} - \mathbf{S}_{Uo})\xi]^{-1} \\ &\quad \times \tilde{P}\boldsymbol{R}_o^{k+1/2}(\lambda) \ .\end{aligned} \tag{A.21}$$

For the isotropic scattering case, the error in the Gauss-Seidel iterate $\boldsymbol{\epsilon}_o^{k+1/2}(\lambda)$ is given by Eq. (A.7). Thus, the modal eigenvalues of our accelerated scheme are determined from the equation:

$$\begin{aligned}\boldsymbol{\epsilon}_o^{k+1}(\lambda) = \Bigg(&\{\mathbf{I} + \xi[\tilde{P}(\lambda^2\mathbf{D} + \mathbf{T} - \mathbf{S}_{Do} - \mathbf{S}_{Uo})\xi]^{-1}\tilde{P}\mathbf{S}_{Uo}\} \\ &\times \left[\mathbf{I} - \frac{1}{\lambda}\tan^{-1}\left(\frac{\lambda}{\mathbf{T}}\right)\mathbf{S}_{Do}\right]^{-1} \\ &\times \frac{1}{\lambda}\tan^{-1}\left(\frac{\lambda}{\mathbf{T}}\right)\mathbf{S}_{Uo} \\ &- \xi[\tilde{P}(\lambda^2\mathbf{D} + \mathbf{T} - \mathbf{S}_{Do} - \mathbf{S}_{Uo})\tilde{X}]^{-1} \\ &\times \tilde{P}\mathbf{S}_{Uo}\Bigg)\boldsymbol{\epsilon}_o^k \ ,\end{aligned} \tag{A.22, A.23}$$

where we have utilized the relation:

$$\boldsymbol{R}_o(\lambda)^{k+1/2} = \mathbf{S}_{Uo}[\boldsymbol{\epsilon}_o^k(\lambda) - \boldsymbol{\epsilon}_o^{k+1/2}(\lambda)] \ . \tag{A.24}$$

The term in brackets in Eq. (A.23) is the Fourier matrix for the two-grid acceleration technique with isotropic scattering, and its eigenvalues determine the convergence rate of the iteration process for a specific Fourier mode λ. Again, the spectral radius is the eigenvalue of largest magnitude obtained for any value of λ.

This analysis can be extended to the P_1 scattering case easily, although it should be noted that only the isotropic component of the flux is being accelerated. Define the matrix $L_3(\lambda)$ as

$$L_3(\lambda) = \begin{bmatrix}\xi[\tilde{P}(\lambda^2\mathbf{D} + \mathbf{T} - \mathbf{S}_{Do} - \mathbf{S}_{Uo})\xi]^{-1}\tilde{P}\mathbf{S}_{Uo} & 0 \\ 0 & 0\end{bmatrix}, \tag{A.25}$$

where 0 is the null matrix. Recalling that Eq. (A.12) defines the Fourier matrix for the Gauss-Seidel process with linearly anisotropic scattering, the Fourier matrix of the two-grid technique is determined from the relation:

$$\begin{aligned}\begin{bmatrix}\boldsymbol{\epsilon}_0^{k+1}(\lambda) \\ \boldsymbol{\epsilon}_1^{k+1}(\lambda)\end{bmatrix} = &\{L_1^{-1}(\lambda)L_2(\lambda) \\ &- L_3(\lambda)[\mathbf{I} - L_1^{-1}(\lambda)L_2(\lambda)]\}\begin{bmatrix}\boldsymbol{\epsilon}_0^k(\lambda) \\ \boldsymbol{\epsilon}_1^k(\lambda)\end{bmatrix}.\end{aligned} \tag{A.26}$$

By comparing the spectral radius of the Gauss-Seidel and the two-grid operators with linearly anisotropic scattering, the effect of the higher-order moments on the effectiveness of our acceleration scheme may be estimated.

ACKNOWLEDGMENT

This work was performed under the auspices of the U.S. Department of Energy.

REFERENCES

1. T. R. HILL, "ONETRAN: A Discrete Ordinates Finite Element Code for the Solution of the One-Dimensional Multigroup Transport Equation," LA-5990-MS, Los Alamos National Laboratory (1975).

2. J. E. MOREL, E. W. LARSEN, and M. K. MATZEN, "A Synthetic Acceleration Scheme for Radiative Diffusion Calculations," *J. Quant. Spectrosc. Radiat. Transfer*, **34**, 243 (1985).

3. J. E. MOREL and J. M. McGHEE, "An Outer Iteration Acceleration Technique for Time-Dependent Even-Parity S_N Calculations," *Nucl. Sci. Eng.* (submitted).

4. A. V. AVERIN and A. M. VOLOSCHENKO, "Consistent P_1 Synthetic Acceleration Method for Outer Iterations," *Transp. Theory Stat. Phys.* (to be published).

5. R. E. MacFARLANE, "TRANSX-CTR: A Code for Interfacing MATXS Cross-Section Libraries to Nuclear Transport Codes for Fusion-System Analysis," LA-9863-MS, Los Alamos National Laboratory (Feb. 1984).

6. T. A. WAREING, Los Alamos National Laboratory, Personal Communication (1992).

7. M. L. ADAMS and W. R. MARTIN, "Diffusion Synthetic Acceleration of Discontinuous Finite Element Transport Iterations," *Nucl. Sci. Eng.*, **111**, 145 (1992).